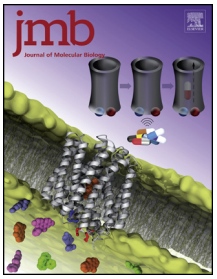

# A New Critical Conformational Determinant of Multidrug Efflux by an MFS Transporter

**Elia Zomot[1,†], Eliane Hadas Yardeni[1,†], Attilio Vittorio Vargiu[2], Heng-Keat Tam[3], Giuliano Malloci[2], Venkata Krishnan Ramaswamy[2], Michal Perach[1], Paolo Ruggerone[2], Klaas Martinus Pos[3] and Eitan Bibi[1]**

***1 - Department of Biomolecular Sciences,*** *Weizmann Institute of Science, Rehovot 76100, Israel*
***2 - Department of Physics,*** *University of Cagliari, 09042 Monserrato (CA), Italy*
***3 - Institute of Biochemistry,*** *Goethe University Frankfurt, 60438 Frankfurt, Germany*

***Correspondence to Eitan Bibi:*** *e.bibi@weizmann.ac.il*
https://doi.org/10.1016/j.jmb.2018.02.026
***Edited by Nieng Yan***

## Abstract

Secondary multidrug (Mdr) transporters utilize ion concentration gradients to actively remove antibiotics and other toxic compounds from cells. The model Mdr transporter MdfA from *Escherichia coli* exchanges dissimilar drugs for protons. The transporter should open at the cytoplasmic side to enable access of drugs into the Mdr recognition pocket. Here we show that the cytoplasmic rim around the Mdr recognition pocket represents a previously overlooked important regulatory determinant in MdfA. We demonstrate that increasing the positive charge of the electrically asymmetric rim dramatically inhibits MdfA activity and sometimes even leads to influx of planar, positively charged compounds, resulting in drug sensitivity. Our results suggest that unlike the mutants with the electrically modified rim, the membrane-embedded wild-type MdfA exhibits a significant probability of an inward-closed conformation, which is further increased by drug binding. Since MdfA binds drugs from its inward-facing environment, these results are intriguing and raise the possibility that the transporter has a sensitive, drug-induced conformational switch, which favors an inward-closed state.


## Introduction

Multidrug (Mdr) transporters are ubiquitous membrane proteins that provide cells with defense against various cytotoxic compounds. They function as multispecific efflux pumps, each able to expel a broad spectrum of chemically dissimilar compounds out of the cell [1]. Bacteria typically harbor numerous Mdr transporter-encoding genes in their genomes [2], which belong to several phylogenetically and mechanistically distinct protein families [3]. Of those, the major facilitator superfamily (MFS) comprises a huge group [3], probably the largest family of transporters [4]. MFS is also the most prominent family of bacterial drug transporters, many of which function as drug/proton antiporters [1].

We study the *Escherichia coli* MFS-related Mdr transporter MdfA, which serves as a model of secondary Mdr transport [5]. Cells expressing MdfA from a multi-copy plasmid exhibit Mdr resistance against a diverse group of unrelated toxic compounds including neutral, zwitterionic, and monovalent cationic ones [2,6]. Transport experiments have shown that MdfA is fueled by the proton electrochemical potential [6–8], and in addition to its drug/proton exchange activity, it may also function as a $(Na^+)(K^+)$/proton antiporter [9]. Clearly therefore, proton translocation by MdfA is crucial for all of its known biological activities. The hypothetical 3D model of MdfA [10] revealed two membrane-embedded negative charges, E26 and D34, which were previously found to be essential for transport of monovalent cationic substrates [11–13] and interaction with protons [14]. Our previous studies have shown that MdfA functionally tolerates displacement of these essential negatively charged side chains to various sites in the putative Mdr recognition pocket [13,15]. Overall, our 3D structural model of MdfA, including

the location of E26 and D34 as well as other important structural features, has been recently confirmed directly in a breakthrough study reporting the high-resolution crystal structure of an MdfA mutant, MdfA(Q131R) [16].

Transporters function by alternating between conformational states; for efficient coupling, the transporter must be able to conformationally respond to interactions with its substrates. In the case of Mdr transporters, this situation is intriguing because they should be able to produce one or more transport-competent conformational responses that fit a variety of chemically and structurally dissimilar substrates. In the past, we studied this question by utilizing several approaches for detecting conformational changes in MdfA and the results suggested that *dissimilar* substrates may induce *similar* conformational changes in MdfA [17]. We proposed that MdfA is structurally very flexible and its conformationally sensitive Mdr recognition pocket responds similarly to dissimilar compounds [17].

Conformational flexibility might explain why MdfA has been so impervious to forming ordered crystals, and up to date, no high-resolution crystal structure has been described for the unconstrained wild-type protein. In contrast, as mentioned above, a recent breakthrough in MdfA studies revealed that a single mutation in MdfA [MdfA(Q131R)] has made it possible to obtain highly ordered crystals that diffracted X-ray down to a resolution of 2 Å [16]. Another recent study demonstrated that Fab fragment-stabilized MdfA is also able to form ordered crystals [18]. In wild-type MdfA, residue Q131 is located at the cytoplasmic side of the proposed Mdr recognition pocket, and together with other residues, it constitutes the rim around the entrance to the pocket from the cytoplasm (Fig. 1). The cytoplasmic rim is electrostatically asymmetric as only one half of the circle is positively charged (Fig. 1). Replacing Q131 by an arginine partially disrupts the charge asymmetry and thus might lead to electrostatic repulsion between the two halves of the rim and possibly stabilization of MdfA(Q131R) in a specific, partially inward-open conformation [16]. To examine this possibility and further characterize the cytoplasmic rim, we investigated the properties of MdfA (Q131R) and additional mutants. Overall, our results revealed that MdfA(Q131R) is almost inactive against the tested MdfA substrates. Similarly, other positive charge insertions in the rim also inhibited MdfA activity, suggesting that electrostatic repulsion might partially limit the drug-induced conformational response of MdfA. Surprisingly, our results also suggest that, unlike the conformation of MdfA(Q131R) in the crystal, the native membrane-embedded wild-type MdfA assumes a relatively stable inward-closed conformation, which is further stabilized by its substrates and a ligand. We propose that the cytoplasmic rim of the Mdr recognition pocket of MdfA plays an important role in drug recognition, transport activity and the conformational behavior of this transporter.

## Results and Discussion

### Properties of MdfA(Q131R)

We first asked whether the crystallized mutant MdfA(Q131R) [16] retains Mdr resistance activity, drug transport, and drug binding. MdfA(Q131R) was expressed as well as wild-type MdfA (Fig. 2a), and cells expressing the mutant or wild-type MdfA were subjected to drug resistance assays (Fig. 2b and c). The results of a typical experiment, which was reproduced numerous times, show unequivocally that MdfA(Q131R) confers very little resistance

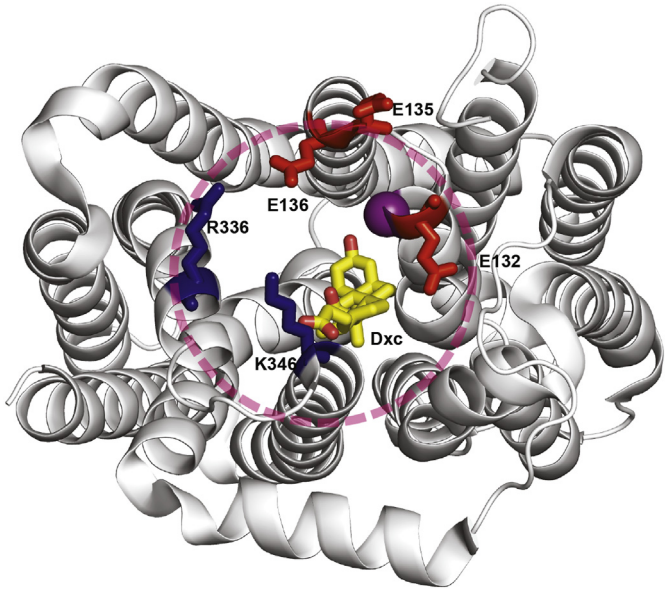


**Fig. 1.** Distribution of charged residues around the intracellular rim of MdfA. The crystal structure of MdfA (Q131R) as viewed from the cytoplasm (4ZP0.pdb) with the proposed intracellular rim (discontinuous pink circle). Basic and acidic residues (blue and red, respectively) located at the rim and facing the cytoplasmic entrance and bound DXC (yellow), are shown as sticks. The Cα atom of the arginine introduced at site 131 is shown as a purple sphere.

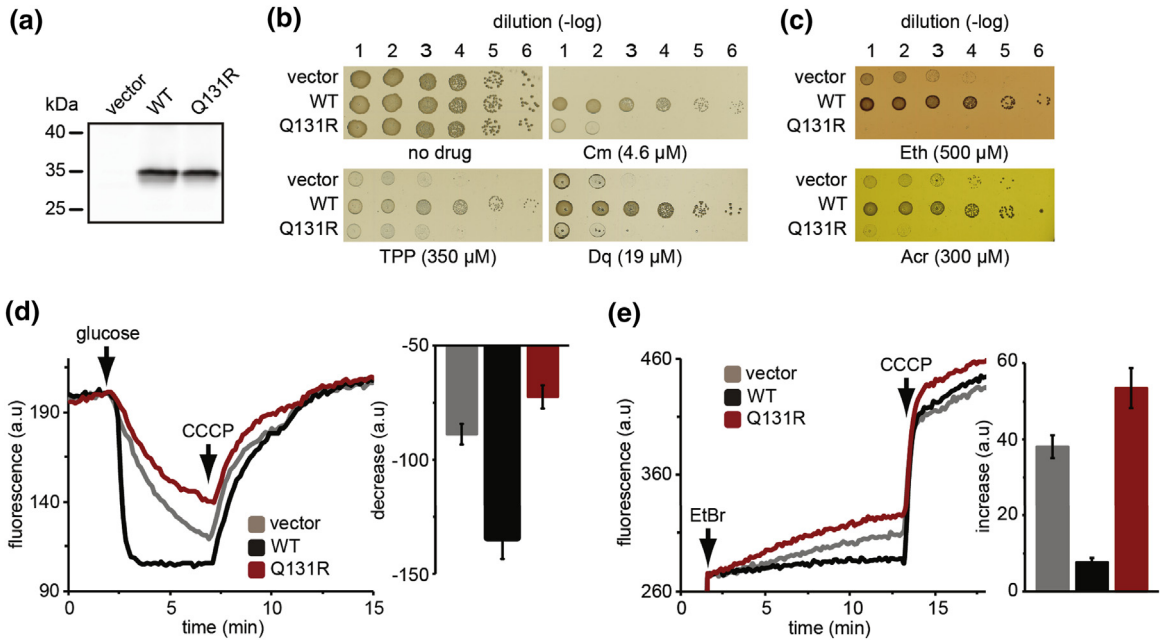


**Fig. 2.** Characterization of expression and activity of MdfA(Q131R). (a) Western blotting analysis of membrane expression of *E. coli* UTL*mdfA*::*kan* transformed with pT7–5 without or with MdfA or MdfA(Q131R). (b, c) Mdr resistance activity of the indicated constructs spotted on LB-agar plates containing the indicated drugs. Eth efflux (d) and influx (e) were monitored continuously by following the fluorescence in whole cells expressing the indicated proteins. Arrows indicate the time of addition of 0.2% glucose (d), 25 μM Eth (e) or 100 μM CCCP (d, e). (d, e) Representative traces (left panels) and averages ± SEM (right panels) from at least four biological smears, each measured in duplicates.

against chloramphenicol (Cm) and no resistance whatsoever against the other tested MdfA substrates, including ethidium (Eth) bromide, tetraphenylphosphonium (TPP) (Table S1), dequalinium (Dq) and acriflavine (Acr). Intriguingly, close inspection of the drug resistance results revealed that instead of resistance, MdfA(Q131R) confers Eth and Acr *sensitivity* (Fig. 2c), suggesting that it might facilitate influx instead of efflux of Eth and Acr. This notion was examined by Eth efflux (Fig. 2d) and influx (Fig. 2e) assays. The efflux experiment showed that wild-type MdfA removed Eth from cells rapidly and cells with empty vector exhibited low efflux activity, probably due to other Mdr transporters. In contrast to cells expressing wild-type MdfA, those expressing the mutant MdfA(Q131R) removed Eth from the cell even more slowly than cells without MdfA (Fig. 2d), suggesting that the mutant might facilitate Eth influx. This was confirmed by the influx assay where unlike wild-type MdfA, which prevented Eth influx almost completely, the mutant MdfA(Q131R) accumulated Eth even more efficiently than cells with no MdfA (Fig. 2e). These results raised the possibility that MdfA (Q131R) indeed permits import of Eth (and Acr) that is driven solely by its own concentration gradient. Since Eth binds the bacterium DNA with a high affinity [19], the actual intracellular concentration of free Eth is kept very low. Therefore, the concentration gradient of the free cationic Eth compound remains stable, enabling efficient influx through MdfA(Q131R), which is also driven by the electrical potential (inside negative). These results evoked the question why other positively charged compounds, such as TPP, cannot move freely through MdfA(Q131R). Since structurally, unlike Eth and Acr, TPP is not a planar compound, one possibility would be that only cationic, planar aromatic compounds may exhibit properties that allow their leakage through MdfA(Q131R). Further insight into the proposed constitutive movement of planar compounds through MdfA(Q131R) was obtained by *in silico* docking studies with Eth and also with the non-planar substrate TPP.

Initially, we assessed the robustness of our docking protocol by re-docking deoxycholate (DXC) into MdfA (Q131R) (PDB ID: 4ZP0) [16]. Several high-affinity docking poses featured small RMSD values from the crystal structure (1.4–2.2 Å), suggesting that the protocol is robust enough in reproducing experimental data (Fig. S1). Next, we performed docking with drugs and the results show that in the wild-type protein and in MdfA(Q131R), the binding of TPP and Eth occurs mostly between the center of the Mdr recognition pocket, lined by residue D34 and the rim around the inward face of the pocket (Fig. 3a–d). Binding of TPP is mostly confined to the center of the Mdr recognition pocket in both the wild type and the mutant (Fig. 3a and b, respectively). In contrast, and only with MdfA(Q131R), Eth has several, relatively high-affinity

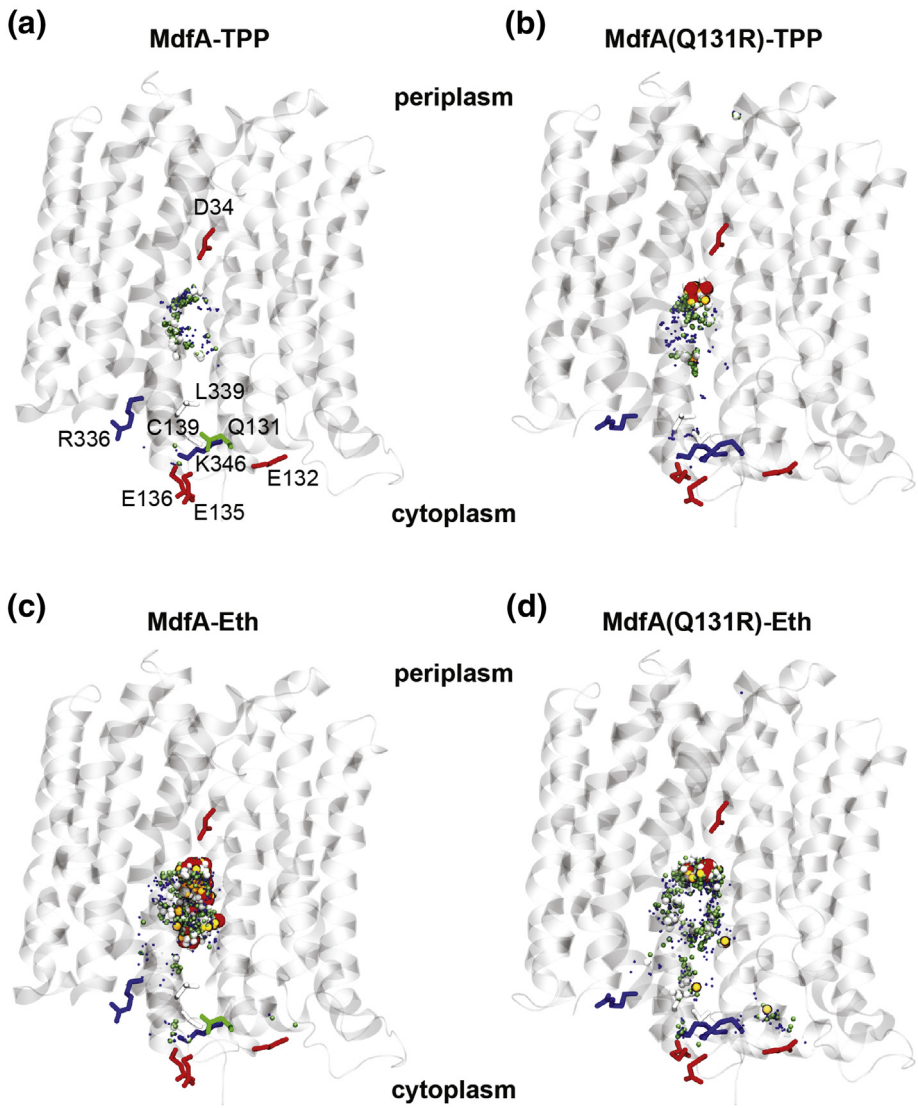


**Fig. 3.** *In silico* docking analyses of TPP and Eth with MdfA and MdfA(Q131R). Comparison between the spatial distributions of the docking poses predicted for TPP (a, b) and Eth (c, d) along the translocation path going from the rim to the center of MdfA for both wild-type (left) and Q131R (right). The centers of mass of the docked poses are represented with spheres of radius increasing with binding affinity and colored according to the following color-code: <−8.5 kcal/mol, blue; <−9.0 kcal/mol, green; <−9.5 kcal/mol, white; <−10.0 kcal/mol, orange; <−10.5 kcal/mol, red. All relevant residues lining the rim as well as D34 are highlighted in licorice and colored by residue type.

poses over a distance of more than 20 Å, from the rim to the protonatable site at position 34 (Fig. 3d). This difference between the localized binding of TPP and the relatively delocalized binding of Eth in MdfA (Q131R) is consistent with the ability of only Eth to diffuse through MdfA(Q131R) from the periplasm to the cytoplasm.

The *in vivo* results with the cationic, non-planar aromatic compound TPP are also interesting, because MdfA(Q131R) does not seem to functionally interact with this compound; it neither confers resistance nor sensitivity to TPP. This raised the possibility that the mutant might not bind TPP or that it binds but is unable to transport this compound. To address this, we first analyzed the theoretical energetics of interaction of TPP with MdfA and MdfA(Q131R) as derived from the *in silico*-docking studies. The docking setup utilized multiple configurations of TPP and of MdfA or MdfA (Q131R), extracted from μs-long molecular dynamics (MD) simulations (see later). In total, we performed 500 independent docking runs [10 configurations of TPP and 50 of MdfA or MdfA(Q131R)], while keeping only the top 5 docking poses from each run. The average binding affinities obtained are reported in Table 1. In terms of average binding affinity of TPP, the results show that MdfA and MdfA(Q131R) are very

**Table 1.** *In silico* substrate-docking energetics

| Substrate | MdfA | | MdfA(Q131R) | |
|---|---|---|---|---|
| | Top 5 | Top 1 | Top 5 | Top 1 |
| TPP | −8.1 ± 0.7 | −8.4 ± 0.7 | −8.4 ± 0.7 | −8.8 ± 0.7 |
| Eth | −8.9 ± 0.7 | −9.4 ± 0.7 | −9.0 ± 0.7 | −9.5 ± 0.7 |

Comparison between the average "pseudo"-binding affinities (in kcal/mol) extracted from the systematic docking campaign for TPP and Eth with MdfA and MdfA(Q131R). Shown are data obtained from both the whole set of docking poses (Top 5) and from the best poses only (Top 1) of each run.

similar, suggesting that the TPP-binding activity of the mutant is retained.

To investigate further the interaction of the mutant with TPP, we purified MdfA and MdfA(Q131R) and compared their TPP-binding activities (Fig. 4a), utilizing equal amounts of protein (Fig. 4b). The equilibrium binding assay showed clearly that MdfA (Q131R) binds TPP very poorly at a concentration of 1 μM, even in the presence of Cm, which is known to enhance the binding of TPP in the case of wild-type MdfA [20]. We next measured the affinity of MdfA (Q131R) to TPP and the results show that its affinity is comparable to that of the wild-type protein (Fig. 4c), as also observed in the *in silico* docking studies (Table 1). Therefore, TPP-binding affinity does not explain why MdfA(Q131R) is unable to confer TPP resistance. Notably, however, in the time window of the experiment where we followed a well-characterized protocol (20 min at 4 °C), only ~15–25% of the MdfA(Q131R) molecules bound TPP even at high TPP concentrations (50 μM, Fig. 4c). The same results were obtained when we examined time-dependent binding (Fig. 4d). One obvious reason could be that a large portion of the purified MdfA(Q131R) is inactive under the experimental conditions. Thus, the TPP-binding experiments with purified MdfA(Q131R) do not offer an answer to why the membrane-embedded mutant is unable to confer TPP resistance. A possible interpretation would be that MdfA(Q131R) is unable to produce a transport competent conformational response upon binding of TPP.

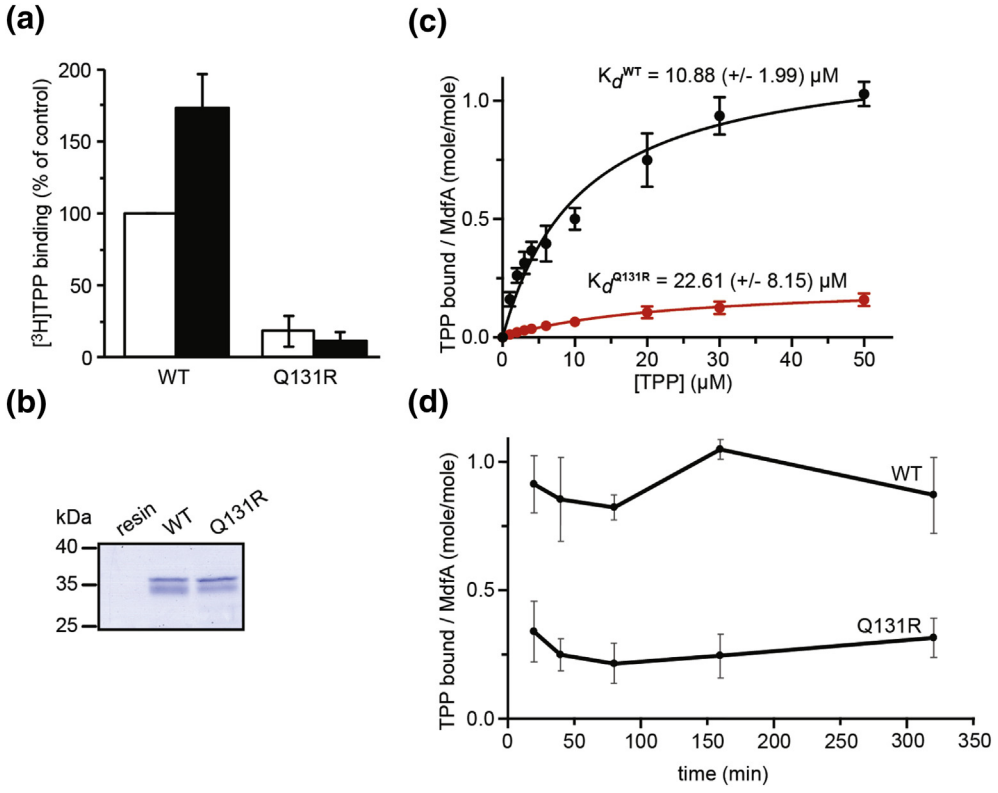


**Fig. 4.** Equilibrium TPP binding with MdfA and MdfA(Q131R). (a) Equilibrium binding assay with 1 μM [$^3$H]TPP in the absence and presence of 0.5 mM Cm (empty and black bars, respectively). (b) Equal-volume samples were taken from the resin used for binding assays, without or with MdfA or MdfA(Q131R) and analyzed by SDS-PAGE and Coomassie blue staining. (c) Binding of [$^3$H]TPP to MdfA and MdfA(Q131R) was measured in the presence of increasing concentrations of TPP. Calculated $K_d$ values are indicated. Experiments were repeated three (a) and five times (b) and values shown are averages ± SEM. Calculated values of Bmax were 1.225 ± 0.08 and 0.226 ± 0.008, and goodness of fit ($R^2$) 0.975 and 0.996, respectively for MdfA and MdfA(Q131R). (d) Time-dependent binding assay in the presence of excess [$^3$H]TPP (50 μM) was performed with MdfA and MdfA(Q131R).

The results presented above suggest that inserting an arginine at position 131 exerts the following effects: (i) Inhibition of the Mdr resistance activity of MdfA. We speculate that the mutation might prevent the productive drug-induced conformational response of MdfA (Q131R), which in the wild-type protein may trigger the closure of the cytoplasmic rim and the opening of the periplasmic face. (ii) Promotion of downhill influx of planar aromatic compounds through MdfA(Q131R) from the periplasm to the cytoplasm. If our hypothesis that MdfA(Q131R) is stabilized in a certain conformation is true, it means that this conformation allows constitutive movement of certain planar compounds through the transporter. Docking studies with MdfA (Q131R) (Fig. 3d) partially support this notion because they show that, in the cytoplasmically oriented Mdr recognition pocket, the planar molecule Eth has several binding poses over a distance of more than 20 Å in MdfA(Q131R).

The hypothesis of electrostatic interactions between Q131R and other charges in the cytoplasmic rim implies that only positively charged residues would lead to this phenotype if inserted at position 131 of MdfA. To address this, residue Q131 of MdfA was replaced by several amino acids, including positively charged (K), negatively charged (D, E), uncharged with a small side chain (A) or with a bulky side chain (H, M, W). Figure 5a shows that all the mutants are expressed as well as wild-type MdfA. Cells expressing each mutant were then examined by drug resistance assays and the results show that all the mutations affected MdfA activity to some extent (Fig. 5b). However, only a positive charge at position 131 (R or K) had a pronounced inhibitory effect on MdfA activity against all the tested compounds (Fig. 5b, framed rows). This supports the notion that increasing the positive charge in the cytoplasmic rim of the Mdr recognition pocket dramatically influences MdfA function. Interestingly, the MdfA(Q131R)-mediated sensitivity to cationic, planar aromatic compounds Eth and Acr was not reproduced in the case of MdfA (Q131K). This might be the result of differences between the lysine and arginine side chains in length, hydrophilicity and/or flexibility. These experiments lend further support to our suggestion that increasing the positive charge in the cytoplasmic rim might lead to stabilization of an inactive conformation, possibly due to repulsion between positively charged residues on opposite sites around the rim.

### Attempts to reverse the phenotype of mutation Q131R by neutralizing basic residues on the opposite side of the rim

As mentioned above, the cytoplasmic rim of the Mdr recognition pocket in MdfA is electrostatically

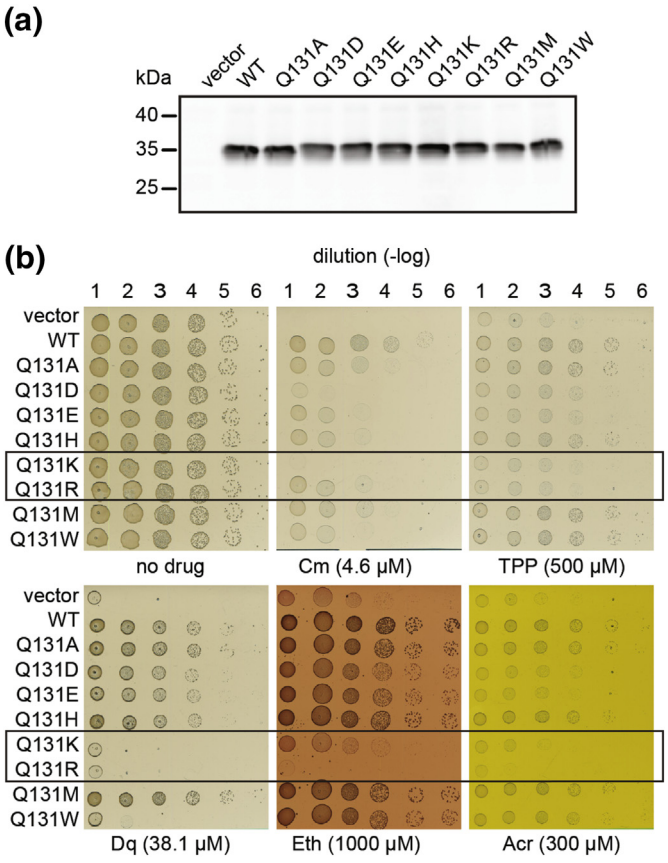


**Fig. 5.** Characterization of MdfA with various substitutions at position 131. Western blotting analysis (a) and Mdr resistance activity (b) of the mutants spotted on LB-agar plates containing the indicated drugs. At least three biological repeats were performed and the results shown are representative.

asymmetric. Mainly, there are two residues, R336 and K346, that are located on the opposite side of the rim compared to residue Q131 (Fig. 6a) and its flanking acidic residues E132 and E136 (Fig. 1). We therefore asked whether it is possible to restore the function of MdfA(Q131R) by neutralizing any one of the two cationic residues and thus reducing the overall positive charge in the rim. In the background of the wild-type MdfA, neutralizing K346 [MdfA(K346Q)] had almost no effect on the resistance activity, while neutralizing R336 [MdfA(R336Q)] inhibited the activity against Cm but not Eth and TPP (Fig. S2). These phenotypes suggest that although increasing the positive charge in the rim was harmful (Fig. 5), reducing it only slightly affected MdfA function, possibly because of secondary effects of the mutations on the substrate recognition profile of the transporter. Next, we created the double mutants MdfA(Q131R/K346Q) and MdfA(Q131R/R336Q) (locations of sites 131, 346 and 336 are shown in Fig. 6a), and observed that their expression was similar to that of MdfA(Q131R) (Fig. 6b). The results of drug resistance assays showed that neutralizing R336 [MdfA(Q131R/R336Q)] largely restored the function of MdfA(Q131R), but only against Cm and TPP. In contrast, neutralizing residue K346 [in MdfA (Q131R/K346Q)] had no effect whatsoever (Fig. 6c), suggesting that only R336 (and not K346) is directly involved in the defective activity of MdfA(Q131R). Moreover, it is interesting that both double mutants retained the Eth and Acr *sensitivity* as observed with MdfA(Q131R) (Fig. 6c). These results reinforce our previous suggestion that the impaired function of MdfA(Q131R) might be caused by electrostatic repulsion between the two positively charged residues, which might stabilize the transporter in a partially inactive conformation.

## Positive charges inserted around the cytoplasmic rim have similar effects on MdfA activity as Q131R

Next, we asked if the specific location of the inserted positive charge (position 131) is crucial for the observed phenotypes or whether decorating other sites around the rim with a positive charge would have similar effects. To answer this, we produced four mutants, each carrying a newly inserted positive charge at a different location around the rim, all of them roughly pointing toward the center of the imaginary rim cycle (Y127R, C139R, I140R, L339R) (Fig. 7a). As controls, we inserted an arginine at position 133 (S133R), which points to an opposite direction (out of the pocket), and at position 279 (T279R), which is located relatively far from the center of the pocket (Fig. 7a). All the mutants were expressed as well as wild-type MdfA (Fig. 7b) and drug resistance assays demonstrated that except Cm in some cases, mutants MdfA(Y127R), MdfA (C139R), MdfA(I140R) and MdfA(L339R) were unable to confer Mdr resistance (Fig. 7c). In contrast, the control mutants MdfA(S133R) and MdfA(T279R) were functional against most of the drugs (Fig. 7c). These results further support our conclusion that MdfA does

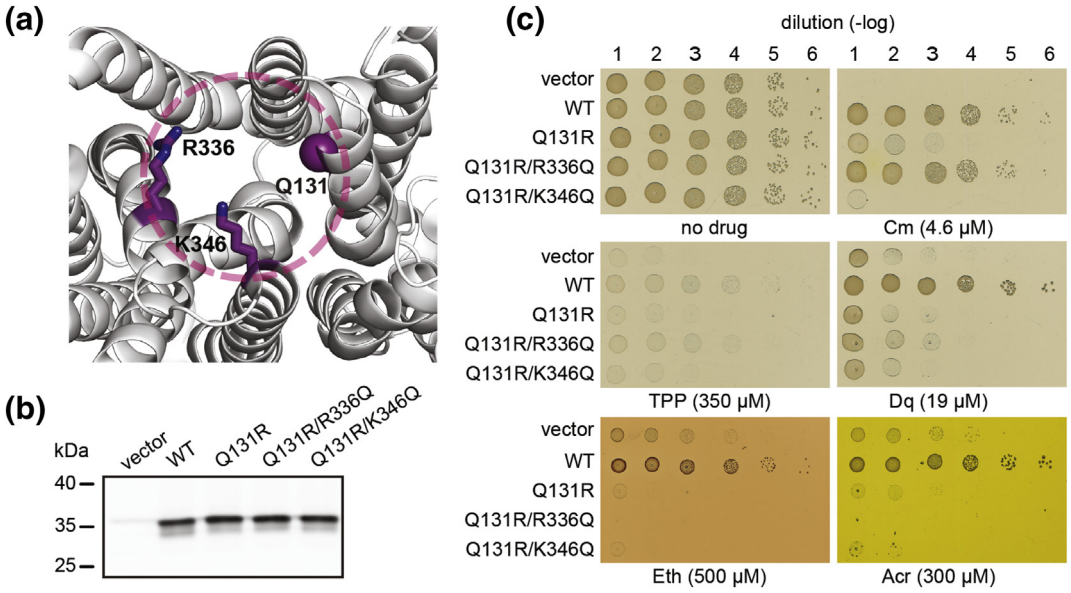


**Fig. 6.** Expression and activity of MdfA(Q131R) neutralized at site 336 or 346. (a) The imaginary cytoplasmic rim is shown as a discontinuous pink circle on a trimmed MdfA(Q131R) structure (4ZP0.pdb), viewed from the cytoplasm. The neutralized positively charged residues are shown as purple sticks. The Cα atom of the arginine introduced at site 131 is shown as a purple sphere. Western blotting analysis (b) and Mdr resistance activity (c) of the mutants spotted on LB-agar plates containing the indicated drugs. At least three biological repeats were performed and the results shown are representative.

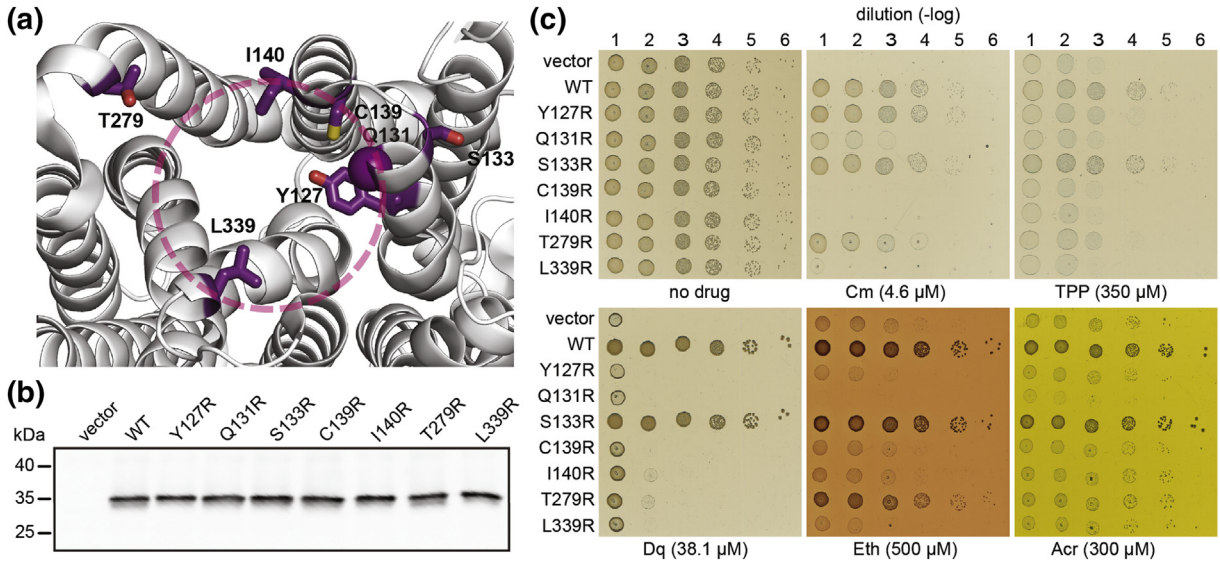


**Fig. 7.** Characterization of MdfA mutants with arginine insertions on the intracellular side. (a) The imaginary cytoplasmic rim is shown as a discontinuous pink circle on a trimmed MdfA(Q131R) structure (4ZP0.pdb), viewed from the cytoplasm. The modified residues are shown as purple sticks. The Cα atom of the arginine introduced at site 131 is shown as a purple sphere. Western blotting analysis (b) and Mdr resistance activity (c) of the mutants spotted on LB-agar plates containing the indicated drugs. At least three biological repeats were performed and the results shown are representative.

not tolerate an increase in the positive charge around the cytoplasmic rim of the Mdr recognition pocket and the effect of the mutation Q131R is representative of this more general phenomenon.

In addition to analyzing the drug resistance profiles of the mutants, we looked for those mutants that might have conferred *sensitivity* to planar cationic drugs. The results show that mutant MdfA(L339R) was able to confer very low, but appreciable and reproducible sensitivity to Eth and Acr (Fig. 7c). However, we were unable to record MdfA(L339R)-mediated Eth-influx (data not shown). In any case, this was interesting because the high-resolution crystal structure of MdfA (Q131R) shows that residues 131 and 339 are located on opposite sides of the cytoplasmic rim, pointing toward each other (Fig. 7a), although the exact orientation of the side chain at position 131 is unknown due to unresolved electron density map in this region of the protein (4ZP0.pdb). These results and those of other manipulations (Figs. 2, 5 and 6) suggest that the cytoplasmic rim has an important role in regulating the activity of MdfA and that in some cases, increasing the overall positive charge in the rim seems to limit the productive conformational response of the transporter and enables constitutive influx of planar, positively charged, aromatic compounds.

## Investigating the effect of a negative charge at position 339 on the phenotype of MdfA(Q131R)

As shown above (Fig. 7), MdfA(L339R) and MdfA (Q131R) exhibit similar properties, as both are defective in their Mdr resistance activity. The two sites, 131 and 339, are located on opposite faces of the cytoplasmic rim around the Mdr recognition pocket (Fig. 7a), at a distance that would allow long-range electrostatic attraction if opposite charges were inserted in these sites. To test this, we used the two mutants with an arginine at either position 131 or position 339 and inserted a glutamate at the opposite location of 339 or 131, respectively [MdfA(Q131R/L339E) and MdfA(Q131E/L339R)]. Both mutants were expressed properly (Fig. 8a) and resistance assays showed that they lost their activity against all tested drugs (Fig. 8b). Notably, the L339E mutation in MdfA(Q131R/L339E) also abolished the Eth and Acr sensitivity seen with the single mutant MdfA(Q131R). These results support the idea that in the double mutants, salt bridges between the oppositely charged residues at positions 131 and 339 might have formed and locked the protein in an inactive conformation. If this is true, a charge pair might also change the overall conformation from inward-open, as proposed for MdfA(Q131R) [16], to an inward-closed conformation. To examine this hypothesis, we crystallized the double mutant MdfA (Q131R/L339E) and solved its structure at a 2.2-Å resolution (PDB ID: 6EUQ), utilizing a similar protocol that was used for purification and crystallization of MdfA(Q131R) [16]. Surprisingly, in the crystal, this mutant has a structure that is almost identical to that of MdfA(Q131R) with DXC (RMSD ~ 0.2 Å) (Fig. 8c), and also here the electron density of the residue at positions 131 (and also 339 in the double mutant)

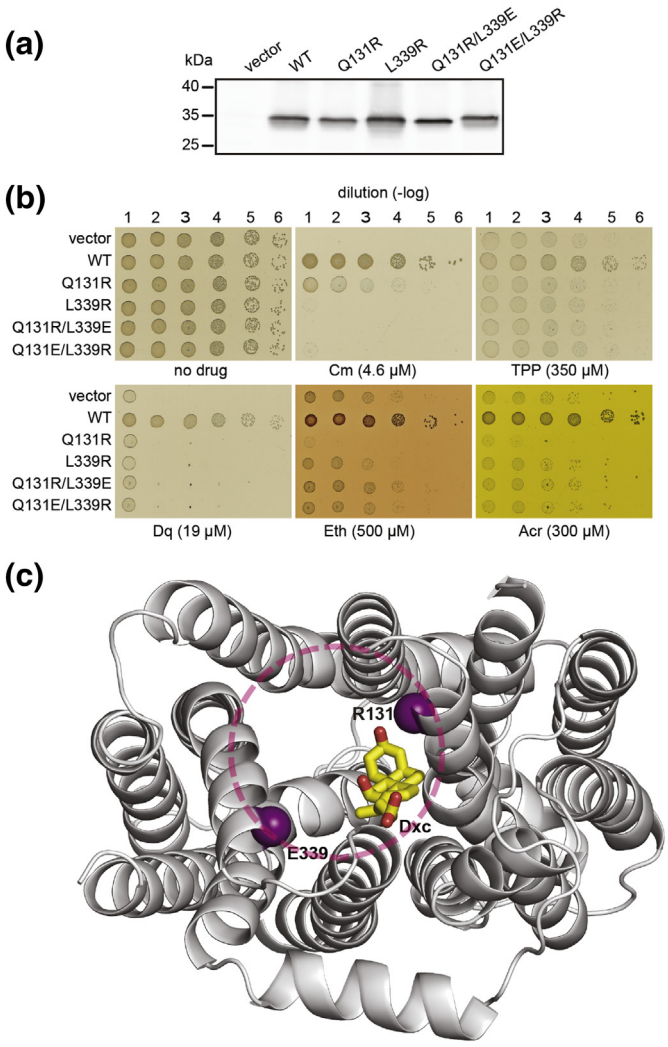


**Fig. 8.** Expression and activity of MdfA mutants at sites 131 and 339 and the crystal structure of MdfA(Q131R/L339E). Western blotting analysis (a) and Mdr resistance activity (b) of the mutants spotted on LB-agar plates containing the indicated drugs. At least three biological repeats were performed and the results shown are representative. (c) X-ray crystal structure of MdfA(Q131R/L339E) obtained at a resolution of 2.2 Å, as viewed from the cytoplasm. The imaginary cytoplasmic rim is shown as a discontinuous pink circle, the DXC bound in the central cavity is shown as yellow sticks, and the Cα atoms of arginine at position 131 and glutamate at 339 are shown as purple spheres.

could not be resolved. These results indicate, contrary to our hypothesis, that in the crystal, the arginine at position 131 does not form a salt bridge with the glutamate at position 339. However, one cannot exclude the possibility that a charge pair does exist in the native membrane-embedded protein or even in its soluble purified form. If this is true, then we should consider the possibility that the crystal structures of MdfA(Q131R) and MdfA(Q131R/L339E) might be dramatically affected by external factors used for purification/crystallization. A likely candidate could be DXC, as this negatively charged amphipathic molecule is occluded within MdfA(Q131R) and MdfA(Q131R/L339E), and present in both crystal structures with its acidic part pointing toward the cytoplasmic rim (Figs. 1 and 8c, respectively). To test the hypothesis that DXC has a dominant role in stabilizing a crystallized conformation that might be entirely different from that of the membrane-embedded MdfA, we performed MD simulations and cross-linking studies.

## All-atom MD simulations suggest that MdfA assumes a relatively stable inward-closed conformation

Having a comprehensive description of the conformational behavior of membrane-embedded MdfA is crucial for better understanding the underlying mechanism of its Mdr transport activity. Therefore, the possibility that the membrane-embedded forms of wild-type and variants of MdfA assume conformations

**Table 2.** Simulated systems

| System | Wild type | Q131R | Q131R/L339E | Q131R/L339E-DXC |
|---|---|---|---|---|
| Number of replicas | 10 | 10 | 10 | 10 |

In all cases, the protein was embedded in a model POPE bilayer and immersed in a 0.1 M KCl water solution. Each simulation replica was extended to 1 μs (production phase).

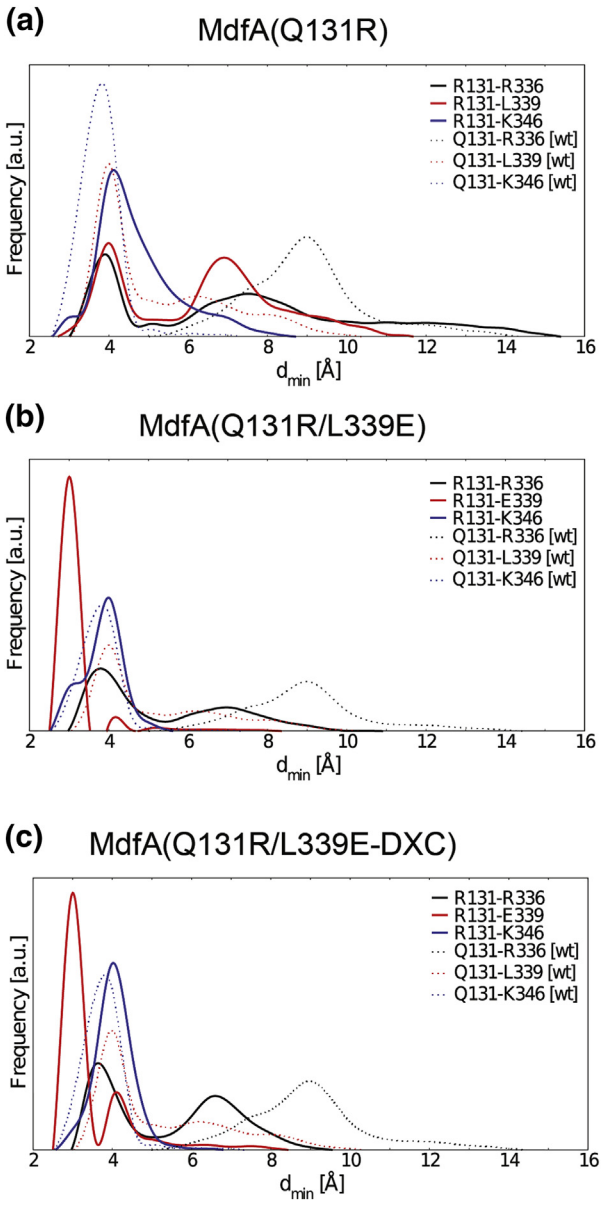


**Fig. 9.** Distribution of minimum distances between putative key residues in the cytoplasmic rim of MdfA mutants. MdfA (Q131R) (a), MdfA(Q131R/L339E) (b), and MdfA(Q131R/L339E) with bound DXC (c). The corresponding distances measured in the wild-type protein are shown as colored dotted lines. Distributions for each system were calculated on the cumulative dataset generated by concatenating the corresponding equilibrium trajectories reported in Table 2.

that are different from those detected in the crystal structures was assessed by performing a series of all-atom 1-μs-long MD simulations of the protein, embedded in a model POPE bilayer, and in the presence of explicit KCl water solution. We simulated four different systems, namely, the wild-type MdfA protein and the variants Q131R, Q131R/L339E and Q131R/L339E in complex with DXC [MdfA(Q131R/L339E-DXC)] (Table 2). In all simulations, the starting conformation was the crystal structure of MdfA(Q131R) (4ZP0.pdb), mutated manually at specific positions when necessary (see Methods). One general significant outcome of the simulations was that all forms of MdfA fluctuate (to different degrees) among various conformations (Fig. S3). This is exemplified for instance by the analyses of selected distances between residues sitting on opposite sides of the rim (Fig. 9). This finding is reasonable, as flexibility is a typical property of Mdr transporters, including MdfA. An important question was whether during the simulation, MdfA(Q131R) diverges from the starting crystal-structure conformation or not, particularly concerning the accessibility to the Mdr recognition pocket through the cytoplasmic rim. The simulation revealed that the 131–339 minimum distance in this system fluctuates mainly between ~4 Å and ~7 Å, suggesting two major conformations of the rim. The results also show that MdfA(Q131R) shifts toward a conformation where the average distance between key residues lining the inward-facing rim is reduced, compared to the analogous estimated distances in the crystal structure (Fig. 9a). Moreover, a clear collapse toward ~3 Å (between residues 131 and 339) was observed when a glutamate was introduced at position 339 (Fig. 9b and c). Therefore, unlike the crystal structures of MdfA (Q131R-DXC) and MdfA(Q131R/L339E-DXC), our models suggest that the inward-closed conformations of these mutants are relatively stable. This finding is supported by the analysis of water-filled regions across the putative translocation pathway (Table 3 and Fig. 10), showing a decrease in the average radii of this pathway that ends at the cytoplasmic rim in MdfA(Q131R/L339E) and MdfA(Q131R/L339E-DXC). Note that the presence of DXC does not have a significant effect on the closure of the rim in the double mutant Q131R/L339E, suggesting this to be an intrinsic feature of the protein embedded in a phospholipid bilayer. Furthermore, these results support the hypothesis that mutations at the rim are structurally coupled to more extended conformational changes and have a large impact on the overall dynamics of the protein, thus on its function.

**Table 3.** Percentage of conformations featuring an open cytoplasmic rim

| System | Wild type | Q131R | Q131R/L339E | Q131R/L339E-DXC |
|---|---|---|---|---|
| % Population with rim open (approx.) | 48% | 56% | 24% | 40% |

The values refer to the fraction of conformations with an open cytoplasmic rim (pore radius >1.15 Å calculated with the program HOLE2). Calculations were performed on the top clusters accounting for nearly 90% of the conformations sampled during the MD simulations (see Methods).

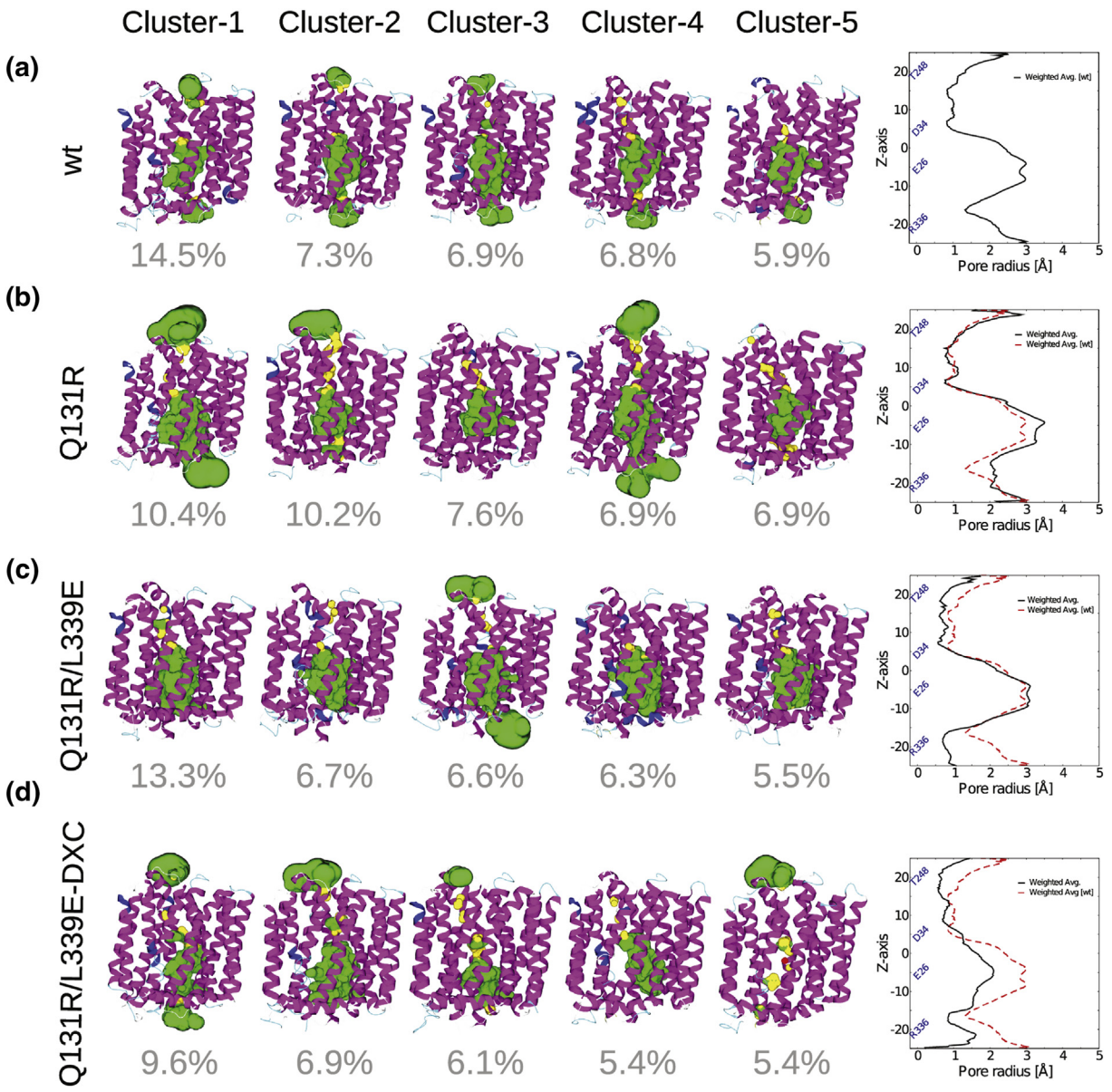


**Fig. 10.** Profiles of the solvent-accessible pathway in the most populated clusters' conformations sampled during the MD simulations of the different MdfA systems. The views are from the lateral sides for every cluster conformation and the corresponding relative population of the cluster is also specified. The protein is shown in cartoon representation colored according to its secondary structure (magenta for helix, blue for $3_{10}$ helix and cyan for turn). The channel surface is colored according to its pore radius: red and yellow identify respectively the parts inaccessible and accessible to water (pore radius <1.15 Å and between 1.15 and 2.3 Å), while green identifies wide areas (pore radius >2.3 Å). The pore-size profile generated with the HOLE2 program is shown on the right side of every panel, with the thick black line representing the population-weighted average radius of the channel for the system being considered and the red dashed line representing that of the wild-type for reference.

## Cross-linking studies reveal that membrane-embedded MdfA assumes a DXC- and substrate-stabilized, inward-closed conformation

To assess the conclusions extracted from mutagenesis data and MD simulations and to roughly estimate the distance between positions 131 and 339 in the native, membrane-embedded MdfA, we performed steady-state cross-linking experiments. An active cysteine-less (CL) MdfA variant [21] was utilized, where we inserted two cysteines to create an active CL-MdfA(Q131C/L339C) (Fig. S4). Initially, we examined whether the double cysteine mutant can form a disulfide bond. Membranes were prepared

from cells expressing the mutant and incubated with copper(II)–phenanthroline (Cu/Ph), which catalyzes disulfide bond formation between very close cysteines. Disulfide bonds are usually detected by SDS-PAGE separation, because they affect the compactness of proteins and limit denaturation under SDS conditions. The more compact (cross-linked) forms sometimes tend to migrate faster on the gel (Fig. 11). Our results show that CL-MdfA does not form a disulfide bond, as expected (Fig. 11a), while mutant CL-MdfA(Q131C/L339C) was able to form a disulfide bond, especially in the presence of Cu/Ph (Fig. 11b), and substrates (TPP and Dq) further facilitate the reaction (Fig. 11b, right panel, and Fig. 11c). Unexpectedly, DXC appears to greatly enhance disulfide bond formation in CL-MdfA(Q131C/L339C) even in the absence of Cu/Ph (Fig. 11d, left panel). In all cases, the disulfide bond can be readily reduced by β-mercaptoethanol (β-Me), as representatively shown in the right panels of Fig. 11c and d. These results suggest that the membrane-embedded MdfA is able to form a relatively stable inward-closed conformation that is further stabilized by substrates and by DXC. This finding is striking, considering that in the crystal structure, the backbone Cα atoms of the two residues at sites 131 and 339 are located ~16 Å apart and the formation of a disulfide bond requires that the distance between the SH groups of the cysteines be ~2 Å. We next tested whether the cross-link is specific to this cysteine pair, by constructing and characterizing another active mutant, CL-MdfA(Q131C/R336C) (Fig. S4). The results clearly show that this pair, located at about the same distance as the former, is also able to form a disulfide bond. Moreover, the cross-linking is substantial without Cu/Ph even in the absence of substrates (Fig. 11e, left panel), and in this case, β-Me only partially reduced the cross-link (Fig. 11e, right panel). This demonstrates that the distance between the cytoplasmic ends of TM4 and TM10 can be very short, as would be expected if MdfA

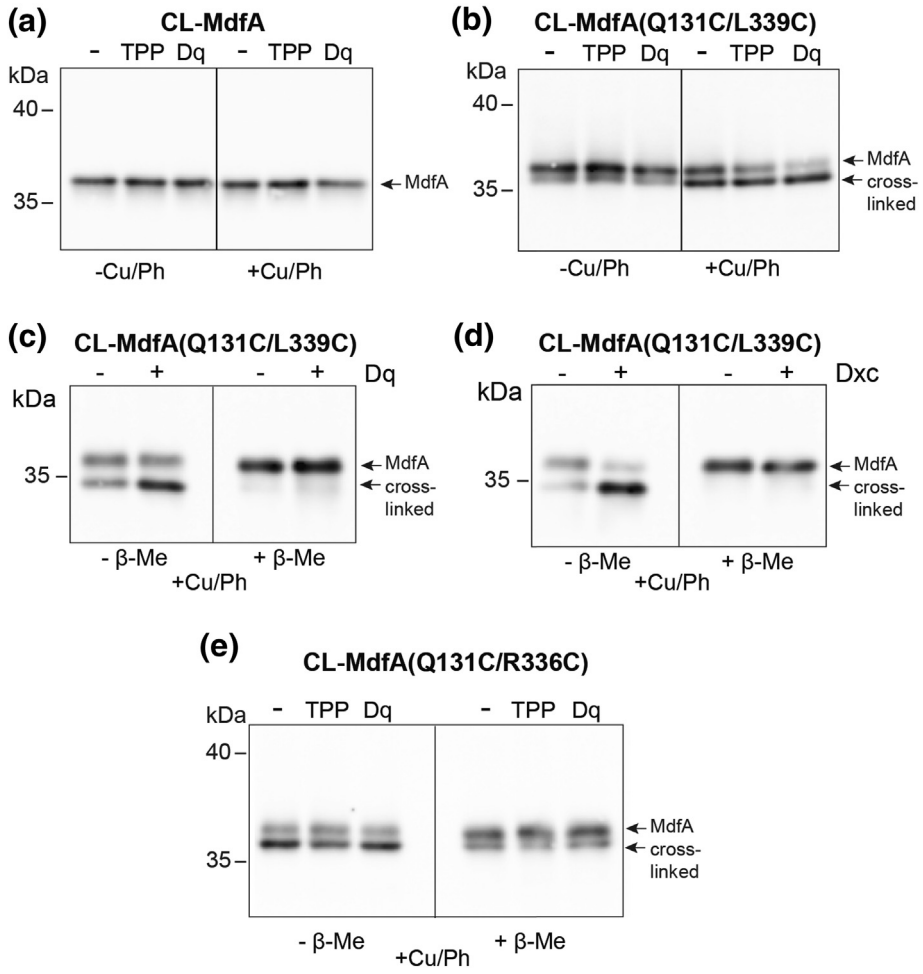


**Fig. 11.** Disulfide bond formation in the cytoplasmic side of MdfA. Membranes from cells expressing CL-MdfA (a), CL-MdfA(Q131C/R339C) (b, c, d) or CL-MdfA(Q131C/R336C) (e) were incubated with or without drugs (or DXC in panel d) and with or without Cu/Ph and analyzed by Western blotting.

assumes an inward-closed conformation. Our results indeed indicate disulfide bond formation, by utilizing a functional split version of MdfA (N6C6c) (Fig. 12a and b). We created a CL version of that split MdfA construct and inserted the same double cysteine mutations [termed CL-N6C6c(Q131C/L339C)]. Figure 12c shows that the two halves of the split protein form a disulfide bond; the cross-linked protein migrates on SDS-PAGE similar to the CL non-split MdfA (CL-MdfA) and β-Me reduces the disulfide bond.

Together, the cross-linking results strongly suggest that the membrane-embedded MdfA(Q131C/L339C) favors an inward-closed conformation, which is entirely different from that found in the crystal structure of MdfA(Q131R/L339E) (Fig. 8c). In the DXC-bound crystal structure, the distance between sites 131 and 339 is greater than 10 Å, whereas the distance between these two residues in the membrane-embedded MdfA(Q131C/L339C) must be compatible with a disulfide bond formation (~2 Å), in good agreement with findings from MD simulations, where a clear peak centered around ~3 Å is seen for both MdfA(Q131R/L339E) and MdfA(Q131R/L339E-DXC) (Fig. 9c and d). Moreover, it is interesting that DXC and MdfA substrates further stabilize this inward-closed conformation, which is opposite to what was expected from the crystal structure of the DXC-bound MdfA(Q131R).

In summary, the notion that the inward-closed conformation of membrane-embedded MdfA is further stabilized by DXC (and drug substrates) is largely supported by our mutagenesis studies, cross-linking results and MD simulations. The observed effect of DXC is of a special interest because it is entirely opposite to its expected effect as seen in the crystal structures of MdfA(Q131R) [16] and MdfA(Q131R/L339E) (Fig. 8c), where it seems to partially open the cytoplasmic rim around the Mdr recognition pocket. Both cases, however, suggest that DXC may be a substrate for MdfA, as has been shown for its *E. coli* homolog MdtM [22], although so far no negatively charged compounds were found to functionally interact with MdfA.

## Conclusions

Crystallization and high-resolution structure determination of MdfA(Q131R) [16] have been extremely important for better understanding the general organization and helix packing in the secondary Mdr transporter MdfA. In addition, the structure raised important mechanistic questions concerning the conformational behavior of this very flexible transporter. More specifically, the site of the mutation that allowed crystallization (Q131R) drew our attention to the possibility that the cytoplasmic rim around the Mdr recognition pocket of MdfA might play an essential role in Mdr transport. Here, we investigated this possibility and indeed observed that certain rim properties are essential for function. The results suggest that increasing the overall positive charge of the rim largely shifts the dynamical equilibrium among different conformations of MdfA toward inactive structural states featuring a constitutively open pathway for influx of planar cationic drugs and thus drug sensitivity.

Our studies of the effect of increasing the positive charge in the cytoplasmic rim also indirectly revealed that the native, membrane-embedded MdfA can assume a relatively stable inward-closed conformation that is entirely different from that observed in the MdfA (Q131R) crystal structure. This finding is even more intriguing because the results show that MdfA substrates, as well as DXC, further increase the probability of the proposed inward-closed conformation, suggesting that antiporters may behave differently from at least several MFS co-transporters that assume a stable inward-open conformation, which then opens on the outside in the presence of substrates [23]. Notably, however, assessing this hypothesis requires direct structural information about MdfA with bound drug in an occluded and/or outward-open conformation.

## Methods

### Strains, plasmids and mutants

Plasmids for overexpression of MdfA-6His or various mutants have been previously described [11–13,20,21]. All mutants were generated utilizing standard PCR methods with mutagenic oligonucleotide primers and plasmids encoding MdfA-6His as a template. All plasmids were sequenced to verify that only the desired mutation was inserted.

### Protein expression analysis

Overnight cultures of *E. coli* UTL2*mdfA::Kan* harboring empty vector or expressing MdfA or variants were diluted and grown to an $A_{600}$ of 0.8–1. Cells were harvested, and membranes were prepared as described previously [24]. Membrane fractions (10 or 20 μg of protein) were then subjected to 12.5% (w/v) SDS/PAGE, electroblotting and detection using India HisProbe-horseradish peroxidase (Pierce) and ECL.

### Drug resistance assay

Antibacterial resistance was assayed as described [13]. Briefly, *E. coli* UTL2*mdfA::Kan* harboring empty vector or expressing MdfA were grown aerobically to $A_{600}$ of ~1 and a series of 10-fold dilutions was prepared. Four microliters of the serial dilution was spotted on drug-containing LB-agar plates and tested for growth after overnight incubation at 37 °C. Minimal

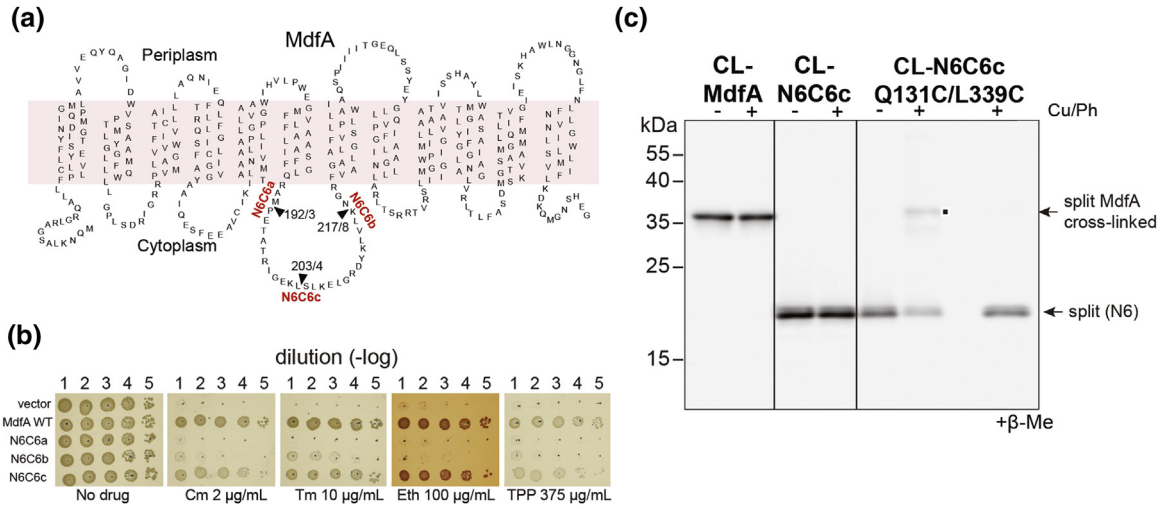


**Fig. 12.** Disulfide bond formation in the cytoplasmic side of an active split MdfA. (a) Secondary structure of MdfA. Arrows indicate location of the splits used to determine optimum split sites. The constructs contain a C-terminal half tagged with a 6His tag and the N-terminal half with a FLAG tag. Wild-type MdfA contains a 6His tag at its C-terminal end. (b) Drug resistance activity of MdfA split constructs against Cm, thiamphenicol (Tm), Eth and TPP. (c) Membranes from cells expressing CL-MdfA, split CL-MdfA (two left panels), or the double cysteine mutant of split CL-MdfA (right panel) were incubated with or without Cu/Ph or β-Me and analyzed by Western blotting.

inhibitory concentration of antimicrobial drugs was determined according to Wiegand *et al* [25] (Table S1). Briefly, cells were grown as above. From a series of 10-fold dilutions, 5-µL aliquots were spotted on freshly prepared LB-agar plates with a range of drug concentrations. Plates were incubated for 16–20 h at 37 °C and the minimal inhibitory concentration was determined based on the inoculum of ~$2 \times 10^4$ colony-forming units.

## MdfA overexpression and purification for biochemical studies

*E. coli* cells harboring plasmid pUC18/*Para*/*mdfA-6His* or any of the mutated constructs were grown at 37 °C in LB medium supplemented with ampicillin (200 µg/mL). Overnight cultures were diluted to ~0.05 $A_{600}$ units, grown to 0.8 $A_{600}$ units and induced with 0.2% (w/v) arabinose for 18 h at 16 °C. Cell pellets were centrifuged for 30 min at 6000*g* and resuspended in 50 mM KPi (pH 7.3) supplemented with 2 mM $MgSO_4$. DNAse (10 µg/mL) and PMSF (1 mM) were then added and the cells passed three times through a pressure cell homogenizer (Stansted) at 15 kPsi for disruption. Cell debris was removed by centrifugation (15 min, 20,000*g*), and the membranes were collected by ultracentrifugation (1 h, 167,000*g*). The membranes were suspended by homogenization in 20 mM Tris–HCl (pH 8.0), 0.5 M NaCl and 10% glycerol, then snap-frozen in liquid nitrogen and stored at −80 °C.

For MdfA purification, thawed membranes were solubilized by addition of 10% *n*-dodecyl-β-D-maltopyranoside (DDM; Anatrace) to a final concentration of 1.1%. Insoluble material was discarded by ultracentrifugation (30 min, 167,000*g*), and the soluble fraction was mixed with solubilization buffer-equilibrated *Talon* beads (Clontech) (typically 0.5-mL bed volume for 20 mL of thawed membranes). Next, the mixture was agitated for 2 h at 4 °C, and the suspension was poured into a column and washed with 30 column volumes of solubilization buffer. MdfA was eluted in 20 mM Tris–HCl (pH 7.2), 0.5 M NaCl, 10% glycerol, 0.1% DDM and 200 mM imidazole. The protein was then dialyzed overnight against dialysis buffer [20 mM Tris–HCl (pH 7.2), 0.12 M NaCl, 10% glycerol, 0.01% DDM) at 4 °C. Protein concentration was determined by measuring $A_{280}$ (1 mg/mL ~ 2.1 $A_{280}$) [26].

## Measurement of [$^3$H]-TPP binding

Radiolabeled TPP binding was carried out by immobilizing purified MdfA-6His on $Ni^{2+}$ beads (Qiagen), allowing it to bind [$^3$H]-TPP (American Radiolabeled Chemicals) and counting the MdfA-associated radioactivity as described [26]. To determine $K_d$, the data were fitted to the equation $B = (B_{max} \times S)/(K_d + S)$ using nonlinear regression, where $B$ is [$^3$H]-TPP bound to MdfA (mole/mol) and $B_{max}$ is the maximal amount of $B$. Calculation of $K_d$ and nonlinear regression was performed using GraphPad Prism version 7 for Windows, GraphPad Software, La Jolla, CA, USA (www.graphpad.com).

## Eth efflux and influx in whole cells

Overnight cultures of *E. coli* UTL2*mdfA*::*kan* cells harboring plain plasmid (pT7–5) or plasmid

pT7–5/*mdfA-6His* or any of the mutants were diluted 100-fold and grown at 37 °C in LB broth supplemented with ampicillin (100 μg/mL) and kanamycin (30 μg/mL) to $A_{600}$ of ~1 and transferred to ice. Cells were pelleted and washed once with wash buffer [50 mM KPi (pH 7.3), 2 mM $MgSO_4$], centrifuged and resuspended in the same buffer. For efflux measurements, 2 mL of cells at $A_{600}$ of 0.6 was incubated with 5 μM Eth and 100 μM carbonyl cyanide 3-chlorophenylhydrazone (CCCP) for 5 min at 37 °C. Then the cells were spun down, resuspended in the same buffer with 5 μM Eth and transferred to cuvettes for fluorescence measurements. D-(+)-glucose was used to energize transport in cells at 0.2% (w/v) and CCCP at 100 μM for dissipating the proton gradient. For influx measurements, pelleted cells on ice were resuspended in M9 minimal medium to $A_{600}$ of 0.6. K-Lactate of 20 mM (pH ~ 7) was added and the cells were incubated for 5 min at room temperature before starting fluorescence measurements at 37 °C. Eth of 25 μM was used to assay Eth influx and 100 μM CCCP for dissipating the proton gradient. Fluorescence of Eth was assayed using excitation wavelength at 480 nm and emission at 620 nm.

### Cysteine cross-linking

Overnight cultures of UTL2*mdfA::kan* expressing double cysteine MdfA mutants (in a CL background) [15] were grown at 37 °C to 1.0–1.5 $A_{600}$ units. Cells were harvested, resuspended in 50 mM sodium–Hepes buffer (pH 7) and supplemented with 1 mM DTT. Membranes were prepared and collected as described above, resuspended in sodium–Hepes buffer (without DTT) at a protein concentration of ~10 μg/μL, flash-frozen in liquid nitrogen and then stored at −80 °C. Oxidative cross-linking with Cu/Ph was carried out with aliquots of membrane suspension (40 μg in 40 μL of the sodium–Hepes buffer), and performed as previously described [27]. Briefly, membranes were preincubated for 20 min at room temperature with or without 1.25 mM of DXC, 0.5 mM TPP or 0.5 mM Dq. Freshly made Cu/Ph stock (0.5 M) was prepared by mixing 40 μL of 1.25 M 1,10-phenanthroline in 50% ethanol and 60 μL of 250 mM $CuSO_4$. Membranes were incubated with Cu/Ph for 1.5 h at room temperature in the presence of DXC, or for 5 min at 37 °C with TPP or Dq, and the reaction was terminated by 10 mM EDTA in a non-reducing protein sample buffer. Samples (6 μg protein) were then subjected to SDS/PAGE using 15% polyacrylamide in the running gel, and analyzed with Western blot.

### MD simulations

The atomistic 3D coordinates of the wild-type MdfA, as well as of its Q131R/L339E (with and without DXC) variant, were generated using the X-ray structure of the Q131R mutant (PDB ID: 4ZP0 [16]) as a template. Single and double mutations were introduced manually through PyMOL [28], and simulations were carried out using the AMBER16 molecular modeling software [29]. The topology and the initial coordinate files of the proteins were created using the *LEaP* module of AmberTools17. The parameters for DXC were taken from the GAFF force field [30,31], while the missing ones were generated using the modules of the AMBER16 package. In particular, atomic restrained electrostatic potential charges were derived using antechamber, after a structural optimization performed with Gaussian09 [32]. The resulting systems were embedded in 1-palmitoyl-2-oleoyl-sn-glycero-3-phosphoethanolamine (POPE) bilayer patches, solvated with explicit TIP3P water model and neutralized with the required number of randomly placed $K^+/Cl^-$ ions. The ions count was suitably adjusted to account for an osmolarity of 0.1 M KCl. The ff14SB [33] version of the AMBER force field was used to represent the protein systems, while lipid14 [34] parameters were used for the POPE bilayer. Embedding of the protein into a pre-equilibrated POPE bilayer patch was performed using the PPM server [35] and subsequently the CharmmGUI tool [36]. The lipid residue nomenclature was converted from CHARMM to AMBER format using the *charmmlipid2amber.py* script provided with AmberTools. Periodic boundary conditions were used, and the distance between the protein and the edge of the box was set to be at least 30 Å in each direction.

Multi-step energy minimization with a combination of steepest descent and conjugate gradient methods was carried out using the *pmemd* program implemented in AMBER16 to relax internal constrains of the systems by gradually releasing positional restraints. Following this, the systems were heated from 0 to 310 K by a 1-ns heating (0–100 K) under constant volume (NVT) followed by 10 ns of constant pressure heating (NPT) (100–310 K) with the phosphorous heads of lipids restrained along the *z*-axis to allow membrane merging and to bring the atmospheric pressure of the system to 1 bar. The Langevin thermostat (collision frequency of 1 $ps^{-1}$) was used to maintain a constant temperature, and multiple short equilibration steps of 500 ps under anisotropic pressure scaling (Berendsen barostat) in the NPT ensemble were performed to equilibrate the box dimensions. After equilibration, multiple μs-long production simulations were performed for each system (see Table 2; total simulated ~42 μs). A time step of 2 fs was used for pre-production runs, while equilibrium MD simulations were carried out with a time step of 4 fs in the NPT ensemble (using a Monte Carlo barostat) conditions after hydrogen mass repartitioning [37]. Coordinates from production trajectories were saved every 100 ps The particle-mesh

Ewald algorithm was used to evaluate long-range electrostatic forces with a non-bonded cutoff of 9 Å. During the MD simulations, the length of all R–H bonds was constrained with SHAKE algorithm. Trajectory analysis was done using *cpptraj* module of AmberTools17 and VMD1.9.2 [38], and graphs were plotted using the *xmgrace* tool.

A cluster analysis of the MD trajectories was performed using the average-linkage hierarchical agglomerative clustering method implemented in *cpptraj* module of AMBER. Such clustering allowed to reduce the number of structures for some of the analysis performed here, yet retaining the large conformational space sampled along the MD trajectories. The clustering was based on RMSD (cutoff set to 3 Å) of the entire protein, considering heavy atoms only. For each system, the representative structures from each of the 50 top clusters generated in this way were used for the qualitative and quantitative analysis of transport channels using HOLE2 program [39], while the entire trajectories were used for the distance and structural convergence analysis.

### Molecular docking

All molecular docking calculations were performed using the software AutoDock Vina [40]. Protein and ligand input files were prepared with AutoDock Tools [41]. We performed a blind docking search by adopting a cubic volume of 50 Å × 50 Å × 50 Å, which encloses the whole protein. The exhaustiveness of the local search was set to 2048 (default 8). Flexibility of both docking partners was taken into account indirectly by considering ensembles of conformations extracted from 1-μs-long MD simulations. For the ligands, we used the same protocol described previously [42]. For MdfA, we used the cumulative trajectory built-up by concatenating the 1-μs-long MD simulations described above. In particular, for each case, we performed 500 independent docking runs using 10 different configurations for the ligands (TPP and Eth) and 50 for MdfA (wild-type and Q131R variant). The whole protocol was validated by re-docking DXC into the X-ray structure of MdfA(Q131R) (4ZP0.pdb).

### Purification of MdfA(Q131R/L339E) for crystallization

Cells expressing MdfA(Q131R/L339E)-6His construct were grown and membranes prepared as described above. Thawed membranes were solubilized by addition of 10% *n*-decyl-β-D-maltopyranoside (Anatrace) to a final concentration of 0.5% (w/v). Insoluble material was discarded by ultracentrifugation (30 min, 167,000*g*), and the soluble fraction was mixed with solubilization buffer-equilibrated *Talon* beads (Clontech) (typically 0.5-mL bed volume for 20 mL of thawed membranes). Next, the mixture was agitated for 2 h at 4 °C, and the suspension was poured into a column and washed with 30 column volumes of solubilization buffer containing 20 mM Tris–HCl (pH 8.0), 0.5 M NaCl, 10% glycerol, 0.2% *n*-decyl-β-D-maltopyranoside and 5 mM imidazole. The protein was concentrated in the same buffer with 200 mM imidazole to about 10 mg/mL and loaded onto a Superdex-200 10/30 column (GE Healthcare) pre-equilibrated with the size exclusion buffer [20 mM Tris–HCl (pH 8.0), 100 mM NaCl, 5 mM β-Me, 1.2 mM sodium Dxc (omitted in some experiments, as indicated), 0.2%–0.4% *n*-nonyl-β-D-glucopyranoside (Anatrace) and 0.025% LDAO (Anatrace)]. Peak fractions were collected, and the pooled protein sample was concentrated to ~15 mg/mL for crystallization screens.

### Crystallization, diffraction data collection and refinement

Crystals of MdfA(Q131R/L339E) were obtained by hanging drop vapor diffusion at 18 °C within 1–2 weeks. The reservoir contained 50 mM sodium acetate (pH 5.6), 20%–28% (v/v) polyethylene glycol 400, 10 mM praseodymium acetate and 50 mM magnesium acetate. Data set of single crystal was collected on beam line Proxima 2A at the Soleil Synchrotron, Saint-Aubin, France, using an Eiger detector (Dectris), indexed and integrated with XDS [43]. The phases were obtained by molecular replacement with MOLREP [44], using coordinates of MdfA(Q131R) (PDB ID: 4ZOW) [16]. Structural models were built in COOT [45] and refined with REFMAC5 [46]. Structures were validated with MolProbity [47]. In the Ramachandran plots, 100.0% of residues were in allowed regions. The statistics for data collection and refinement are shown in Table S2.

### Data deposition

Crystallography, atomic coordinates and structure factors have been deposited in the Protein Data Bank, www.pdb.org (PDB ID code 6EUQ).

## Acknowledgments

This work was supported by the German–Israeli Foundation for Scientific Research and Development to K.M.P. and E.B. (GIF, Grant No. I-1202-248.9/2012) and the Visiting Scientist program of the Cagliari University and of the Regione Autonoma della Sardegna (legge 7 agosto 2007, n. 7: "Promozione ricerca scientifica e innovazione technologica

in Sardegna") to E.B. E.B. holds the Jerome A., Freda, and Edward M. Siegel Professorial Chair. *In silico* studies are part of the Translocation Consortium (http://www.translocation.eu) with a support from the Innovative Medicines Initiative Joint Undertaking under Grant Agreement no. 115525, the European Union's Seventh Framework Programme (FP7/2007–2013) and EFPIA companies. V.K.R. is a Marie Skłodowska–Curie fellow within the "Translocation" Network, project no. 607694.

**Author Contributions**: E.Z. planned, performed and analyzed experiments. Writing—original draft. E.H.Y. planned, performed and analyzed experiments, and helped in writing the original draft. A.V.V., planned, performed and analyzed MD simulations, and helped in writing the original draft. H.K.T. planned, performed and analyzed crystallization experiments, and helped in writing the original draft. G.M. planned, performed and analyzed docking calculations, and helped in writing the original draft. V.K.R. analyzed *in silico* data and helped in writing the original draft. M.P. planned, constructed and characterized split MdfA constructs. P.R. contributed to the supervision, funding acquisition, data analysis and writing of the original draft. K.M.P. contributed to the conceptualization, supervision, funding acquisition, data analysis and writing of the original draft. E.B. initiated and supervised the project, and contributed to the conceptualization, funding acquisition, project administration, data interpretation and writing of the paper.

**Competing Financial Interests**: The authors declare no competing financial interests.

## Appendix A. Supplementary Data

Supplementary data to this article can be found online at https://doi.org/10.1016/j.jmb.2018.02.026.

*Received 31 January 2018;*
*Received in revised form 20 February 2018;*
*Accepted 27 February 2018*
Available online 9 March 2018

***Keywords:***
MdfA;
multidrug resistance;
multidrug transport;
secondary transport;
major facilitator superfamily

†E.Z. and E.H.Y. contributed equally to this work.

***Abbreviations used:***
Mdr, multidrug; MFS, major facilitator superfamily; Cm, chloramphenicol; Eth, ethidium; TPP, tetraphenylphosphonium; Dq, dequalinium; Acr, acriflavine; DXC, deoxycholate; MD, molecular dynamics; CL, cysteine-less; β-Me, β-mercaptoethanol; DDM, *n*-dodecyl-β-D-maltopyranoside; CCCP, carbonyl cyanide 3-chlorophenylhydrazone; POPE, 1-palmitoyl-2-oleoyl-sn-glycero-3-phosphoethanolamine.

## References

[1] N. Fluman, E. Bibi, Bacterial multidrug transport through the lens of the major facilitator superfamily, Biochim. Biophys. Acta 2009 (1794) 738–747.
[2] K. Nishino, A. Yamaguchi, Analysis of a complete library of putative drug transporter genes in *Escherichia coli*, J. Bacteriol. 183 (2001) 5803–5812.
[3] M.H. Saier Jr., I.T. Paulsen, Phylogeny of multidrug transporters, Semin. Cell Dev. Biol. 12 (2001) 205–213.
[4] M.H. Saier Jr., B.H. Eng, S. Fard, J. Garg, D.A. Haggerty, W. J. Hutchinson, et al., Phylogenetic characterization of novel transport protein families revealed by genome analyses, Biochim. Biophys. Acta 1422 (1999) 1–56.
[5] N. Sigal, D. Cohen-Karni, S. Siemion, E. Bibi, MdfA from *Escherichia coli*, a model protein for studying secondary multidrug transport, J. Mol. Microbiol. Biotechnol. 11 (2006) 308–317.
[6] R. Edgar, E. Bibi, MdfA, an *Escherichia coli* multidrug resistance protein with an extraordinarily broad spectrum of drug recognition, J. Bacteriol. 179 (1997) 2274–2280.
[7] O. Lewinson, J. Adler, G.J. Poelarends, P. Mazurkiewicz, A. J. Driessen, E. Bibi, The *Escherichia coli* multidrug transporter MdfA catalyzes both electrogenic and electroneutral transport reactions, Proc. Natl. Acad. Sci. U. S. A. 100 (2003) 1667–1672.
[8] T. Mine, Y. Morita, A. Kataoka, T. Mizushima, T. Tsuchiya, Evidence for chloramphenicol/H+ antiport in Cmr (MdfA) system of *Escherichia coli* and properties of the antiporter, J. Biochem. 124 (1998) 187–193.
[9] O. Lewinson, E. Padan, E. Bibi, Alkalitolerance: a biological function for a multidrug transporter in pH homeostasis, Proc. Natl. Acad. Sci. U. S. A. 101 (2004) 14073–14078.
[10] N. Sigal, E. Vardy, S. Molshanski-Mor, A. Eitan, Y. Pilpel, S. Schuldiner, et al., 3D model of the *Escherichia coli* multidrug transporter MdfA reveals an essential membrane-embedded positive charge, Biochemistry 44 (2005) 14870–14880.
[11] J. Adler, O. Lewinson, E. Bibi, Role of a conserved membrane-embedded acidic residue in the multidrug transporter MdfA, Biochemistry 43 (2004) 518–525.
[12] R. Edgar, E. Bibi, A single membrane-embedded negative charge is critical for recognizing positively charged drugs by the *Escherichia coli* multidrug resistance protein MdfA, EMBO J. 18 (1999) 822–832.
[13] N. Sigal, N. Fluman, S. Siemion, E. Bibi, The secondary multidrug/proton antiporter MdfA tolerates displacements of an essential negatively charged side chain, J. Biol. Chem. 284 (2009) 6966–6971.
[14] N. Fluman, C.M. Ryan, J.P. Whitelegge, E. Bibi, Dissection of mechanistic principles of a secondary multidrug efflux protein, Mol. Cell 47 (2012) 777–787.
[15] J. Adler, E. Bibi, Promiscuity in the geometry of electrostatic interactions between the *Escherichia coli* multidrug resistance transporter MdfA and cationic substrates, J. Biol. Chem. 280 (2005) 2721–2729.
[16] J. Heng, Y. Zhao, M. Liu, Y. Liu, J. Fan, X. Wang, et al., Substrate-bound structure of the *E. coli* multidrug resistance transporter MdfA, Cell Res. 25 (2015) 1060–1073.

[17] N. Fluman, D. Cohen-Karni, T. Weiss, E. Bibi, A promiscuous conformational switch in the secondary multidrug transporter MdfA, J. Biol. Chem. 284 (2009) 32296–32304.
[18] K. Nagarathinam, F. Jaenecke, Y. Nakada-Nakura, Y. Hotta, K. Liu, S. Iwata, et al., The multidrug-resistance transporter MdfA from *Escherichia coli*: crystallization and X-ray diffraction analysis, Acta Crystallogr F Struct Biol Commun. 73 (2017) 423–430.
[19] M.J. Waring, Complex formation between ethidium bromide and nucleic acids, J. Mol. Biol. 13 (1965) 269–282.
[20] O. Lewinson, E. Bibi, Evidence for simultaneous binding of dissimilar substrates by the *Escherichia coli* multidrug transporter MdfA, Biochemistry 40 (2001) 12612–12618.
[21] J. Adler, E. Bibi, Determinants of substrate recognition by the *Escherichia coli* multidrug transporter MdfA identified on both sides of the membrane, J. Biol. Chem. 279 (2004) 8957–8965.
[22] S. Paul, K.O. Alegre, S.R. Holdsworth, M. Rice, J.A. Brown, P. McVeigh, et al., A single-component multidrug transporter of the major facilitator superfamily is part of a network that protects *Escherichia coli* from bile salt stress, Mol. Microbiol. 92 (2014) 872–884.
[23] M.G. Madej, L. Sun, N. Yan, H.R. Kaback, Functional architecture of MFS D-glucose transporters, Proc. Natl. Acad. Sci. U. S. A. 111 (2014) E719–27.
[24] N. Fluman, J. Adler, S.A. Rotenberg, M.H. Brown, E. Bibi, Export of a single drug molecule in two transport cycles by a multidrug efflux pump, Nat. Commun. 5 (2014) 4615.
[25] I. Wiegand, K. Hilpert, R.E. Hancock, Agar and broth dilution methods to determine the minimal inhibitory concentration (MIC) of antimicrobial substances, Nat. Protoc. 3 (2008) 163–175.
[26] N. Sigal, O. Lewinson, S.G. Wolf, E. Bibi, *E. coli* multidrug transporter MdfA is a monomer, Biochemistry 46 (2007) 5200–5208.
[27] Y. Zhou, M.G. Madej, L. Guan, Y. Nie, H.R. Kaback, An early event in the transport mechanism of LacY protein: interaction between helices V and I, J. Biol. Chem. 286 (2011) 30415–30422.
[28] L. Schrödinger, The PyMOL Molecular Graphics System, 2012 Version 1.5.
[29] D. Case, D. Cerutti, T. Cheatham III, T. Darden, R. Duke, T. Giese, et al., AMBER 16, University of California, San Francisco, 2017.
[30] J. Wang, R.M. Wolf, J.W. Caldwell, P.A. Kollman, D.A. Case, Development and testing of a general amber force field, J. Comput. Chem. 25 (2004) 1157–1174.
[31] J. Wang, W. Wang, P.A. Kollman, D.A. Case, Automatic atom type and bond type perception in molecular mechanical calculations, J. Mol. Graph. Model. 25 (2006) 247–260.
[32] M.J. Frisch, G.W. Trucks, H.B. Schlegel, G.E. Scuseria, M.A. Robb, J.R. Cheeseman, et al., Gaussian 09, Revision A.02, Gaussian, Inc., Wallingford CT, 2016.
[33] J.A. Maier, C. Martinez, K. Kasavajhala, L. Wickstrom, K.E. Hauser, C. Simmerling, ff14SB: improving the accuracy of protein side chain and backbone parameters from ff99SB, J. Chem. Theory Comput. 11 (2015) 3696–3713.
[34] C.J. Dickson, B.D. Madej, Å.A. Skjevik, R.M. Betz, K. Teigen, I.R. Gould, et al., Lipid14: the amber lipid force field, J. Chem. Theory Comput. 10 (2014) 865–879.
[35] M.A. Lomize, I.D. Pogozheva, H. Joo, H.I. Mosberg, A.L. Lomize, OPM database and PPM web server: resources for positioning of proteins in membranes, Nucleic Acids Res. 40 (2012) D370-D6.
[36] S. Jo, T. Kim, V.G. Iyer, W. Im, CHARMM-GUI: a web-based graphical user interface for CHARMM, J. Comput. Chem. 29 (2008) 1859–1865.
[37] C.W. Hopkins, S. Le Grand, R.C. Walker, A.E. Roitberg, Long-time-step molecular dynamics through hydrogen mass repartitioning, J. Chem. Theory Comput. 11 (2015) 1864–1874.
[38] W. Humphrey, A. Dalke, K. Schulten, VMD: visual molecular dynamics, J. Mol. Graph. 14 (1996) 33–38.
[39] O.S. Smart, J.M. Goodfellow, B. Wallace, The pore dimensions of gramicidin A, Biophys. J. 65 (1993) 2455–2460.
[40] O. Trott, A.J. Olson, AutoDock Vina: improving the speed and accuracy of docking with a new scoring function, efficient optimization, and multithreading, J. Comput. Chem. 31 (2010) 455–461.
[41] G.M. Morris, R. Huey, W. Lindstrom, M.F. Sanner, R.K. Belew, D.S. Goodsell, et al., AutoDock4 and AutoDockTools4: automated docking with selective receptor flexibility, J. Comput. Chem. 30 (2009) 2785–2791.
[42] G. Malloci, A.V. Vargiu, G. Serra, A. Bosin, P. Ruggerone, M. Ceccarelli, A database of force-field parameters, dynamics, and properties of antimicrobial compounds, Molecules 20 (2015) 13997–14021.
[43] W. Kabsch, Xds, Acta Crystallogr. D Biol. Crystallogr. 66 (2010) 125–132.
[44] A. Vagin, A. Teplyakov, Molecular replacement with MOLREP, Acta Crystallogr. D Biol. Crystallogr. 66 (2010) 22–25.
[45] P. Emsley, B. Lohkamp, W.G. Scott, K. Cowtan, Features and development of Coot, Acta Crystallogr. D Biol. Crystallogr. 66 (2010) 486–501.
[46] G.N. Murshudov, P. Skubak, A.A. Lebedev, N.S. Pannu, R.A. Steiner, R.A. Nicholls, et al., REFMAC5 for the refinement of macromolecular crystal structures, Acta Crystallogr. D Biol. Crystallogr. 67 (2011) 355–367.
[47] V.B. Chen, W.B. Arendall III, J.J. Headd, D.A. Keedy, R.M. Immormino, G.J. Kapral, et al., MolProbity: all-atom structure validation for macromolecular crystallography, Acta Crystallogr. D Biol. Crystallogr. 66 (2010) 12–21.